I&EC research
Industrial & Engineering Chemistry Research

Article

pubs.acs.org/IECR

Comparative Study of the Adsorption Equilibrium of CO_2 on Microporous Commercial Materials at Low Pressures

S. I. Garcés,[†] J. Villarroel-Rocha,[‡] K. Sapag,[‡] S. A. Korili,[†] and A. Gil*[,†]

[†]Departamento de Química Aplicada, Edificio de los Acebos, Universidad Pública de Navarra, Campus de Arrosadía, 31006 Pamplona, Spain

[‡]Laboratorio de Sólidos Porosos, INFAP, CONICET-Universidad Nacional de San Luis, Chacabuco, 917, 5700 San Luis, Argentina

Supporting Information

ABSTRACT: The adsorption of CO_2 on several microporous materials has been measured at various temperatures (263, 273, 283, and 293 K) over a wide range of pressures. The porous materials studied were three zeolites (5A, 13A, and 13X), two metal−organic frameworks (Basolite A100 and Basolite Z1200), an activated carbon, and two pillared clays (Al-PILC and Zr-PILC). The data obtained were fitted to the Freundlich, Langmuir, and Toth isotherms. Various methods were used to calculate the Henry's law constants. The values found for the zeolites, which ranged from 8.95 to 36.02 mmol/kPa·g at 273 K, were much higher than those for the metal−organic frameworks, activated carbon, and pillared clays, which ranged from 0.012 to 0.200 mmol/kPa·g at the same temperature. The isosteric heats of adsorption of CO_2 on the materials were calculated using the Clausius−Clapeyron equation, and the adsorbent−CO_2 affinity was found to increase in the order Z1200 ≈ 13X ≈ 13A < 5A < Zr-PILC < A100 ≈ AC ≈ Al-PILC at low loadings.

1. INTRODUCTION

The ever-increasing global population and degree of industrialization mean that energy consumption is growing rapidly. Indeed, according to recent forecasts, energy demand will increase by 53% by 2035.[1] As fossil fuels still remain the predominant energy source, emissions of anthropogenic CO_2 must be reduced to control this source of greenhouse gas.[2]

Carbon capture and storage (CCS) from flue gas is a valuable option for reducing CO_2 emissions into the atmosphere that has received considerable attention in recent years.[3−5] Current CCS schemes employ a series of technologies for the capture of CO_2, followed by its compression, transport, and permanent storage. In this context, absorption, adsorption, membrane separation, and cryogenic methods have been developed to separate and capture CO_2. CCS methodologies also complement other strategies, such as switching to lower-carbon fuels, improving energy efficiency, and phasing in the use of renewable energy sources.

Although physical and chemical absorption using aqueous solutions of alkanolamine or chilled ammonia are currently used[6] for the large-scale capture of CO_2, this process suffers from several drawbacks that hamper its implementation, including high energy consumption, equipment corrosion, toxicity, poor chemical stability, poor mass-transport efficiency, and flow problems caused by viscosity.[7] To reduce the costs of capturing CO_2, alternative techniques have focused on research into innovate materials with high adsorption capacities and high selectivities for use in adsorption technologies involving electrical-, pressure-, temperature-, or vacuum-swing-based adsorption systems.[8] The solid adsorbents considered for use in CO_2 capture because of their high adsorption capacities include zeolites,[9−16] activated carbons,[9,17−22] amine-functionalized mesoporous silicas,[23] hydrotalcite,[24,25] hydroxy metal carbonates,[26] and metal−organic frameworks (MOFs).[27−30] However, systematic comparisons of CO_2 capture using several adsorbents have rarely been reported in the literature. Some of the properties that such porous materials must present include a highly reversible CO_2 adsorption capacity at ambient pressures and temperatures; rapid kinetics; a low H_2O adsorption capacity at low partial pressures of H_2O; high selectivity for CO_2 over H_2O and N_2; complete regenerability with a low heat of adsorption, thus allowing for easy regeneration at moderate temperatures; stability over a large number of cycles; good hydrothermal stability with high attrition resistance; high bulk density; and low cost.

Activated carbons have been proposed to be the most suitable materials for CO_2 capture as their adsorption performance is dependent on their pore structure and their surface chemical properties.[31] Although the capture capacities of activated carbons are, in general, lower than those of zeolites at low pressure and under ambient conditions, activated carbons present a series of advantages as CO_2 adsorbents, such as higher capacities at higher pressures, ease of regeneration, low cost, and low moisture sensitivity.[32] Other types of carbonaceous sorbents have also been considered for CO_2 capture.[33,34]

Both zeolites and active carbons have traditionally been used in separation technology, especially pressure-swing-adsorption (PSA) processes.[9,23,35−38] The most widely used such material is probably the zeolite 13X, which is the main adsorbent for commercial hydrogen production using PSA[39] and can also be used to recover CO_2 from a binary mixture.[40] However, although zeolites are known to be suitable for PSA applications,

Received: January 31, 2013
Revised: April 2, 2013
Accepted: April 28, 2013
Published: April 28, 2013

dx.doi.org/10.1021/ie400380w | Ind. Eng. Chem. Res. 2013, 52, 6785−6793

their regeneration requires significant energy input,[4] and they tend to be more expensive than carbonaceous adsorbents.

MOFs are a new type of porous material with unique structural properties. As such, they have received a great deal of attention because of their large surface areas, tunable pore sizes, and large accessible pore volumes, which confer them with significant advantages over traditional adsorbents such as zeolites.[30,41,42] These adsorbents are therefore ideal for applications in gas adsorption and storage.[43−45] In the specific case of CO_2 capture and storage, the selectivity of zeolitic imidazolate frameworks (ZIFs) has been highlighted.[46−48] However, the industrial application of MOFs is restricted by their low thermal stability compared to zeolites and carbonaceous adsorbents. In contrast to many MOFs, the MIL (Materials of the Institut Lavoisier) series of frameworks and ZIFs exhibit high thermal stabilities.[4,49] Other solid materials of interest as a result of their high surface areas and important role as sorbents in environmental applications are pillared interlayered clays (PILCs),[50] which have also found widespread use as catalytic supports. Although the preparation and characterization of these materials has been widely reported, few studies have investigated their ability to retain and separate gases.[51−54]

Adsorption equilibrium and kinetic studies are essential during the design, simulation, and development of separation processes and are currently used to provide information when characterizing the type of adsorbent−adsorbate interactions involved. Likewise, such studies are also essential when validating and developing models and theories to describe the behavior of such processes. In this sense, adsorption equilibrium, isosteric heat, and kinetic data are used to evaluate the adsorption capacity, selectivity, and adsorbent selection parameters for the storage, separation, and purification of gases and gas mixtures.[55,56] Although adsorption equilibrium data for several gases on zeolites, activated carbons, and MOFs have been extensively reported, to the best of our knowledge, very few data are available for CO_2 under the conditions used herein. Furthermore, none of the previous reports involved a systematic study of several types of microporous commercial adsorbents under the same conditions.

The aim of this work was therefore to undertake a systematic study of the adsorption equilibrium of CO_2 on three zeolites, two MOFs, an activated carbon, and two pillared clays at near-room temperatures and low pressures to provide valuable information that could be useful when selecting appropriate adsorbents for economical storage, as well as to provide reliable adsorption equilibrium data, which are currently not available in the open literature for some of these materials.

2. EXPERIMENTAL SECTION

2.1. Materials. The porous adsorbents used in this work were commercial materials, including three synthetic zeolites (5A, 13A, and 13X), two MOFs (A100 and Z1200), an activated carbon (AC), and two synthetic pillared clays (Al-PILC and Zr-PILC).

2.1.1. Zeolites. The structure of zeolite A consists of eight sodalite cages located at the corners of a cube and joined through a four-membered oxygen ring. This arrangement forms a large polyhedral α cage with a free diameter of about 1.14 nm that can be accessed through eight-membered oxygen windows. The stacking of these units in a cubic lattice gives a three-dimensional isotropic channel structure that is constricted by the eight-membered oxygen rings.[57] Zeolites 5A (Fluka) and 13A (Merck) are the calcium and sodium forms of molecular sieves and present pore sizes of 0.5 and 1.0 nm, respectively.

Zeolite X presents a faujasite-type framework structure that can be thought of as a tetrahedral lattice of sodalite units connected through six-membered oxygen bridges or, equivalently, as a tetrahedral arrangement of double six-ring units. The resulting channel structure is open, with each cage connected to four other cages through 12-membered oxygen rings with a free diameter of around 0.74 nm.[57] Zeolite 13X (Sigma-Aldrich) is a sodium-modified molecular sieve with a pore diameter of 0.74 nm.

2.1.2. Metal−Organic Frameworks. Basolite A100 is a Sigma-Aldrich trademark for the MIL-53 MOF. This MOF has a structure built from infinite chains of corner-sharing $MO_4(OH)_2$ octahedra (in this case, M = Al^{3+}) interconnected by dicarboxylate groups.[58] The structure is a tridimensional metal−organic framework containing a single pore size (free diameter close to 0.85 nm) and diamond-shaped channels.[59]

Basolite Z1200 is a Sigma-Aldrich trademark for the ZIF-8 MOF. ZIF (zeolitic imidazolate framework) materials are a subfamily of MOFs in which the crystalline structures composed of metal ions and organic linkers are ordered in a manner similar to that of silicon and oxygen in zeolites. ZIF-8 is composed of $Zn(MeIM)_2$ (MeIM = 2-methylimidazolate) with a sodalite-type structure and exhibits an interesting pore topology. The internal cavities of this material have a diameter of 1.16 nm, with an aperture diameter of 0.34 nm.[47]

2.1.3. Carbon Material. The activated carbon used in this work is sold by Sigma-Aldrich as Darko KB-B. This material is a noncrystalline solid with a slit pore geometry between two graphene layers.

2.1.4. Pillared Interlayered Clays. Inorganic pillared interlayered clays (PILCs) are prepared by exchanging the charge-compensating cations present in the interlamellar space of swelling clays with hydroxy metal polycations. Upon calcination, the inserted polycations yield rigid, thermally stable oxide species that hold the clay layers apart and prevent their collapse. Pillared clays have been used in several applications, such as catalysis, adsorption, and ion exchange.[50] The synthesis of the alumina and zirconia pillared clays used in this work has been reported previously.[60]

2.2. Adsorption Experiments. Nitrogen (Air Liquide, 99.999%) adsorption experiments at 77 K were performed using a static volumetric apparatus (Quantachrome Autosorb-iQ). Carbon dioxide (Air Liquide, 99.998%) adsorption measurements at 263, 273, 283, and 293 K were performed using a different static volumetric apparatus (Micromeritics ASAP 2010 adsorption analyzer). The adsorption temperatures were controlled using a circulating thermostatic bath (Polyscience, model 9702) containing Dynalene HC-50 as the heat-transfer medium. The materials were placed in a sample holder and immersed in a dewar containing the same liquid for precise temperature control. All samples (0.2 g) were degassed for 24 h at 473 K and a pressure lower than 0.133 Pa prior to use.

3. MATHEMATICAL MODELS AND THEORY

3.1. Adsorption Isotherms. Various isotherm equations have been proposed to describe the experimental data from the adsorption of gases on porous materials. In this work, three isotherm equations, namely, the Freundlich, Langmuir, and Toth equations, were used to describe the experimental carbon dioxide adsorption results.[61] The first two equations are widely

dx.doi.org/10.1021/ie400380w | Ind. Eng. Chem. Res. 2013, 52, 6785−6793

used and can be useful for comparison reasons, whereas the Toth equation is more appropriate for heterogeneous microporous solids, as the estimation of its parameters can provide information regarding the heterogeneity of the material. The three isotherm equations used in this work are given by

Freundlich equation

$$C = k_F p^{1/m_F} \tag{1}$$

Langmuir equation

$$C = \frac{C_0 k_L p}{1 + k_L p} \tag{2}$$

Toth equation

$$C = \frac{C_0 k_T p}{[1 + (k_T p)^{m_T}]^{1/m_T}} \tag{3}$$

where C (mmol/g) is the amount adsorbed, C_0 (mmol/g) is the monolayer capacity, k_i is the equilibrium constant (k_F) or the binding affinity (k_L and k_T), and m_i characterizes the heterogeneity of the system and the mobility of the molecules adsorbed.[61] According to Toth,[62] values of m_T higher than 1 are indicatives of heterogeneous surfaces where the adsorbent−adsorbate interactions are greater than those between the molecules adsorbed. The parameters were estimated independently for every temperature by nonlinear regression.

Although the parameters k_i and m_i are temperature-dependent,[61,63] this dependence is complex, and Do proposed that k_F and m_F are not independent. In this work, the temperature dependence of the parameters is described using an Arrhenius-type equation with parameters a_i, b_i, A_i, and B_i

$$m_i = a_i \exp\left(\frac{-b_i}{RT}\right) \tag{4}$$

$$k_i = A_i \exp\left(\frac{-B_i}{RT}\right) \tag{5}$$

3.2. Henry's Constant. This constant is an important characteristic of adsorption because it provides an indication of the strength of adsorption and the isosteric heat of adsorption at low pressure. Various methods for obtaining Henry's constant are presented and compared in this work. Thus, Henry's constant (H) can be obtained directly from the isotherm (limiting slope) if it is linear at the lowest pressure limits. If sufficient low-pressure data are unavailable, the method suggested by Ruthven[64] provides a reliable means for determining H values, using the virial equation of adsorption, expressed as

$$\ln(p/C) = A_0 + A_1 C + A_2 C^2 + \cdots + A_m C^m \tag{6}$$

where A_m represents the virial coefficients, which include horizontal interactions between the adsorbed molecules.[62] A_0 is related to the Henry's constant (H_{virial}) as[65]

$$H_{virial} = \exp(-A_0) \tag{7}$$

Several statistical tools, including the adjusted coefficient of determination, a residuals analysis, and an F test (probability of 5%), were used herein to obtain the number of virial parameters with significance.[66] The best fit was found for six statistically significant coefficients.

The limiting-slope method is more accurate than other methods if sufficient data in the low-pressure regime are available. The virial expression is useful if there is a need to extrapolate the data at lower pressures from the data available at higher pressures.

The product of the parameters C_0 and k_T in the Toth equation also gives Henry's constant (H_{Toth}).[67]

The temperature dependence of the Henry's constant (H_i) can also be described using an Arrhenius-type equation

$$H_i = C_i \exp\left(\frac{-D_i}{RT}\right) \tag{8}$$

where the two parameters C_i and D_i are found by fitting the values obtained at several temperatures.

3.3. Heat of Adsorption. Adsorption leads to temperature changes that can be significant and therefore need to be taken into account when designing an adsorption-based separation process. These heat effects can be described by the isosteric heat of adsorption and can be determined from the amount of gas adsorbed. The isosteric heat defines the energy change resulting from the phase change (gaseous phase to adsorbed phase) of an infinitesimal number of molecules at constant pressure and temperature and a specific adsorbate loading. Thermodynamically, it can be expressed as the difference between the molar enthalpy in the gas phase and the differential enthalpy in the adsorbed phase

$$q_{st} = h^g - \left[\frac{\partial H^m}{\partial n^m}\right]_T \tag{9}$$

where H^m is the specific enthalpy of the adsorbed phase and n^m is the specific amount adsorbed. The superscript m denotes that the variables are measured Gibbs excess variables.[68]

One method that is widely used to calculate the isosteric heat of adsorption involves the application of the Clausius−Clapeyron equation,[68] which relates the isosteric heat to the pressure change of the bulk gas phase as a consequence of a temperature change for a constant amount adsorbed

$$q_{st} = -R\left[\frac{\partial \ln p}{\partial(1/T)}\right]_n \tag{10}$$

where p (kPa) is the equilibrium pressure, n is the amount of gas absorbed at temperature T (K), and R (kJ/mol·K) is the universal gas constant. The use of this equation is based on the assumptions that the bulk gas phase behaves in an ideal manner and that the volume of the adsorbed phase can be neglected. These two assumptions are reasonable at low pressures but might not be true at higher pressures. The isosteric heat can be obtained from the experimental isotherms at various temperatures by plotting ln p versus $1/T$ for a constant loading n. The isosteric heat corresponds to the slope of the straight line.

4. RESULTS AND DISCUSSION

4.1. Textural Properties. The nitrogen adsorption isotherms for all materials studied are shown in Figure 1. Their textural properties are summarized in Table 1. The specific surface areas (S_{BET}) were estimated using the Brunauer−Emmett−Teller (BET) equation[69] according to the criteria suggested by Rouquerol et al.[70] A nitrogen molecule cross-sectional area of 0.162 nm^2 was considered.[69] The total pore volume ($V_{p,T}$) was calculated from the amount of nitrogen adsorbed at a relative pressure of 0.985, assuming that the density of the nitrogen condensed in the pores is equal to that of liquid nitrogen at 77 K (0.81 g/cm^3).[71] The micropore

dx.doi.org/10.1021/ie400380w | Ind. Eng. Chem. Res. 2013, 52, 6785−6793

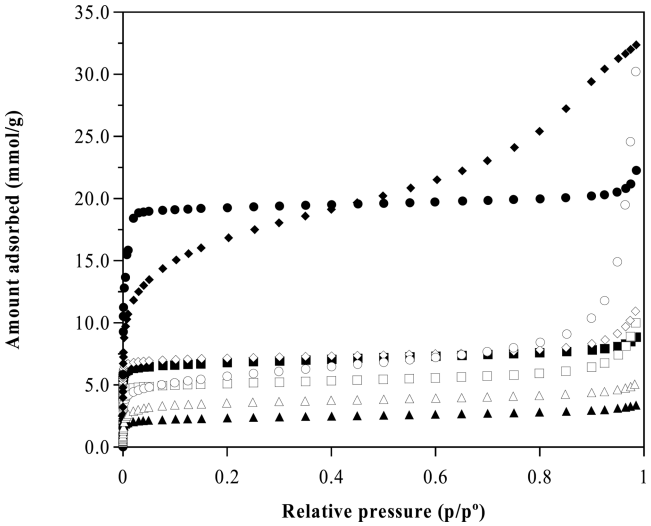

Figure 1. N_2 adsorption on the microporous materials at 77 K: (■) 5A, (□) 13A, (◊) 13X, (○) A100, (●) Z1200, (♦) AC, (▲) Al-PILC, and (Δ) Zr-PILC.

Table 1. Textural Properties Derived from N_2 Adsorption at 77 K and CO_2 Adsorption at 273 K

material	S_{BET}[a] (m^2/g)	$V_{p,T}$[b] (cm^3/g)	$V_{\mu p}(N_2)$[c] (cm^3/g)	$V_{\mu p}(CO_2)$[d] (cm^3/g)
5A	610	0.31	0.20	0.20
13A	460	0.35	0.15	0.22
13X	655	0.38	0.22	0.25
A100	465	1.05	0.13	0.57
Z1200	1925	0.77	0.63	0.37
AC	1370	1.12	0.36	0.35
Al-PILC	200	0.12	0.07	0.10
Zr-PILC	310	0.18	0.10	0.10

[a]Specific surface area calculated using the BET equation. [b]Specific total pore volume at a relative pressure of 0.985. [c]Specific micropore volume obtained by the α_s-plot method. [d]Specific micropore volume derived from the Dubinin–Radushkevich (DR) equation.

volume $[V_{\mu p}(N_2)]$ was calculated using the α_s-plot method,[69] with nonporous hydroxylated silica as the reference adsorbent[72] for 5A, 13A, 13X, Al-PILC, Zr-PILC, A100, and Z1200 materials and the nonmicroporous activated carbon CarbonA as the reference adsorbent[73] for the AC material. The micropore volume $[V_{\mu p}(CO_2)]$ was also calculated using the Dubinin–Radushkevich equation[74] over the relative pressure range 0.01–0.034 for carbon dioxide adsorption at 273 K assuming that the density of CO_2 liquid at 273 K is 1.073 g/cm^3.

From the results presented in Figure 1, the nitrogen adsorption isotherms of the materials under study show the following behavior: (i) a type I isotherm shape (according to the IUPAC classification[75]) at low relative pressure, due to strong adsorbent–adsorbate interactions caused by adsorption in micropores;[71] (ii) at high relative pressures ($p/p°$) up to 0.8, a slight increase in the amount adsorbed in zeolites, MOFs, and PILCs and a more pronounced increase for AC, thus resulting in a combined type I/II isotherm and a plateau that can clearly be seen in the case of Z1200; and (iii) at higher relative pressures ($0.8 < p/p° < 1$), a rapid increase in the amount adsorbed for all materials due to the filling of large mesopores, macropores, or interparticle spaces, especially in the case of sample A100.

A comparison of the specific surface areas (S_{BET}) for all adsorbents listed in Table 1 gives the order Z1200 > AC > 13X > 5A > 13A ≈ A100 > Zr-PILC > Al-PILC. Similarly, the $V_{\mu p}(N_2)$ values for the samples give the order Z1200 > AC > 13X > 5A > 13A > A100 > Zr-PILC > Al-PILC, and the $V_{\mu p}(CO_2)$ values yield the order A100 > Z1200 > AC > 13X > 13A > 5A > Zr- and Al-PILC. In the A100 material, for which $V_{\mu p}(N_2) < V_{\mu p}(CO_2)$, there is a narrow microporosity that cannot be measured with N_2 adsorption. On the contrary, the Z1200 material $[V_{\mu p}(N_2) > V_{\mu p}(CO_2)]$ presents large micropores. In general, the MOF materials present the largest micropore volumes, and the PILC samples present the smallest.

4.2. Carbon Dioxide Adsorption. High-resolution CO_2 adsorption equilibrium isotherms up to 1 atm for all of the solids investigated are presented in Figures 2 and S1 of the

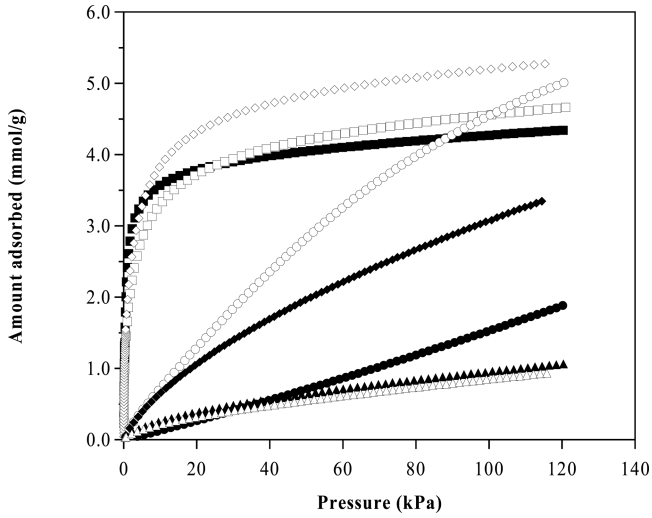

Figure 2. CO_2 adsorption on the microporous materials at 273 K: (■) 5A, (□) 13A, (◊) 13X, (○) A100, (●) Z1200, (♦) AC, (▲) Al-PILC, and (Δ) Zr-PILC.

Supporting Information. As shown in Figure 2, the CO_2 adsorption capacities of the sorbents follow the order 13X > 13A > 5A > A100 > AC > Z1200 > Al-PILC > Zr-PILC, thus showing that the zeolites exhibit higher CO_2 capacities than the other porous solids. These results indicate that the adsorption capacities of the materials depend on both the textural properties, such as specific surface area or pore volume, and the pore-size distribution and formation of carbonate species. Several types of carbonate species could be formed according to the presence of coordinatively unsaturated sites in the neighborhhod and explain the adsorption behavior found. Zeolites exhibit a much narrower microporosity in the ultramicropore region.[76] The CO_2 adsorption capacities of A100 and AC increased much more rapidly with pressure than those of the other materials. In Figure S1 (Supporting Information) are shown the CO_2 isotherms for various temperatures, where it is important to note that, as expected for exothermic processes, the amount adsorbed by each sample decreased with increasing temperature.

The parameters of the Freundlich, Langmuir, and Toth equations were estimated independently for each temperature by nonlinear regression, and the values obtained are presented in Table S1 (Supporting Information). Considering the experimental pressure range as a whole, the experimental points are much better described by the Toth model than by

dx.doi.org/10.1021/ie400380w | Ind. Eng. Chem. Res. 2013, 52, 6785–6793

Table 2. Henry's Constants for CO_2 Adsorption on Microporous Materials at Several Temperatures Obtained Using Three Methods

temperature (K)	H_{virial} (mmol/kPa·g)	H (mmol/kPa·g)	H_{Toth} (mmol/kPa·g)	temperature (K)	H_{virial} (mmol/kPa·g)	H (mmol/kPa·g)	H_{Toth} (mmol/kPa·g)
	5A				Z1200		
263	17.05	17.91	44.64	263	0.016	0.018	0.022
273	10.46	8.95	17.87	273	0.012	0.013	0.019
283	8.94	4.38	9.28	283	0.009	0.010	0.009
293	6.29	2.45	5.02	293	0.007	0.008	0.010
	13A				AC		
263	30.37	16.89	69.43	263	0.204	0.132	0.191
273	14.51	9.06	36.02	273	0.123	0.085	0.104
283	11.92	5.20	23.60	283	0.077	0.055	0.063
293	11.67	2.10	8.32	293	0.051	0.040	0.040
	13X				Al-PILC		
263	11.7	24.19	88.85	263	0.136	0.028	1.000
273	9.44	16.62	33.25	273	0.082	0.021	0.200
283	8.41	10.75	31.19	283	0.049	0.015	0.063
293	4.26	6.57	17.16	293	0.034	0.012	0.036
	A100				Zr-PILC		
263	0.195	0.109	0.103	263	0.204	0.042	2.474
273	0.119	0.070	0.069	273	0.111	0.030	0.151
283	0.076	0.050	0.048	283	0.099	0.022	0.126
293	0.052	0.037	0.048	293	0.062	0.016	0.052

the Freundlich and Langmuir isotherms, thus indicating that the Toth isotherm, which assumes a quasi-Gaussian distribution of surface energy, is more suitable for describing the behavior found. The experimental results also show that the Freundlich isotherm can describe the behavior found for MOFs, activated carbon, and pillared clays because it does not have a finite limit when the pressure is sufficiently high.

The inhomogeneity of the material surface is described by the parameter m in the Freundlich and Toth isotherm equations. m_F is greater than 1, and m_T is less than 1 in all of the materials studied herein (see Table S1, Supporting Information), thus indicating the heterogeneity of the surfaces. The only exception was found for the sample Z1200, although this is most likely due to the homogeneous surface of this material and the linear adsorption isotherm obtained.

Arrhenius-type eqs 4 and 5 were used to describe the temperature-dependence of the parameters k_i and m_i in the Freundlich, Langmuir, and Toth equations. The values of all the parameters, as estimated by nonlinear regression, are given in Table S2 (Supporting Information).

An accurate value for the Henry's law constant is necessary to determine the adsorbate−adsorbent interactions that characterize adsorbent heterogeneity and adsorption affinity. As such, Henry's constants were calculated by the methods presented in section 3.2; the results are summarized in Table 2. A semilogarithmic plot of the isotherms measured at 273 K is presented in Figure S2 (Supporting Information) to magnify the Henry's law regime. Clear differences can be seen among the data obtained using a virial-type isotherm, those obtained in the low-pressure region, and those estimated from the Toth isotherm. The product of the parameters C_0 and k_T in the Toth isotherm allows the Henry's constant to be calculated. However, because these parameters are generally fitted to describe a wide pressure range, the fit between the model and the experiment is not perfect in the low-pressure range in most cases. Additionally, Toth isotherms reduces to Henry's law only if the limiting conditions are: $m_T = 1$ (homogeneous surface) and $k_T p \ll 1$. This explains the differences between the values obtained for the zeolites and for the pillared clays using this method. Only four experimental data points were used to calculate Henry's constant from the adsorption isotherm in the low pressure limits. Although several authors[14,77−82] have suggested that the virial equation provides a reliable method of calculating the Henry's law constant with good accuracy, the polynomial grade used is not fixed in all cases. The same authors also indicated that this approach is simply a polynomial fitting with no starting assumptions regarding the adsorption process but that nevertheless provides a precise extrapolation of the adsorption constant at zero coverage. A comparison of the Henry's law constants for the adsorbents showed that those for the zeolites are higher, thus indicating stronger adsorption on these materials than on the MOFs, activated carbon, or pillared clays. The Henry's law constants at 273 K were in the ranges of 9−36 mmol/kPa·g for the zeolites and 0.01−0.20 mmol/kPa·g for the other materials.

4.3. Isosteric Heat of Adsorption. The isosteric adsorption technique was used to calculate the heats of adsorption to provide information about the interaction between the adsorbate molecules and the adsorbent surfaces. It is also considered to be a sensitive probe for adsorption on nonuniform surface, reflecting the heterogeneity in the distribution of surface energy of the material as well. The isosteric heat, q_{st} (kJ/mol), was calculated from the adsorption isotherms at several temperatures by using the Clausius−Clapeyron expression (eq 10). For these calculations, each isotherm was converted to an adsorption isostere by plotting $\ln p$ as a function of reciprocal absolute temperature $(1/T)$ at a given adsorbed amount (up to 3.5 mmol/g), thus resulting in straight lines from which the isosteric heat could be calculated directly from the slope. These adsorption isosteres can be found in Figure S3 (Supporting Information). The linear behavior obtained shows that the isosteric heat of adsorption is not temperature-dependent in the range investigated and depends only on the amount adsorbed. The dependence of the

dx.doi.org/10.1021/ie400380w | Ind. Eng. Chem. Res. 2013, 52, 6785−6793

isosteric heats of adsorption on the amount adsorbed for the eight adsorbents studied is shown in Figure 3, which clearly

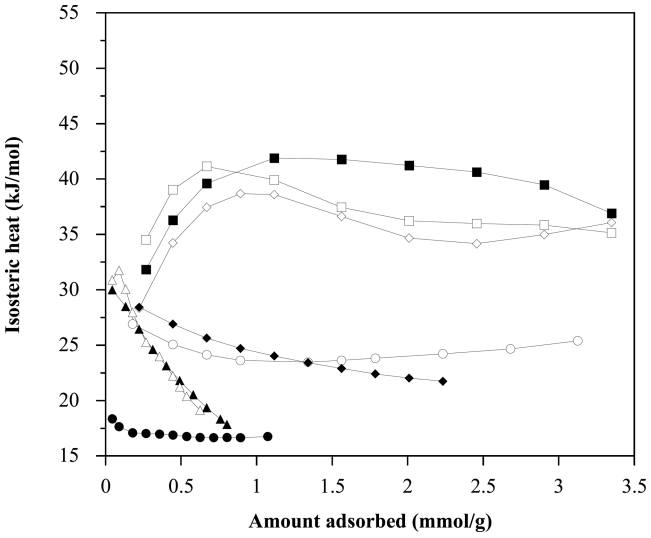

Figure 3. Isosteric heat of CO_2 adsorption as a function of the amount of CO_2 adsorbed on the microporous materials: (■) 5A, (□) 13A, (◊) 13X, (○) A100, (●) Z1200, (♦) AC, (▲) Al-PILC, and (Δ) Zr-PILC.

indicates that the isosteric heats of adsorption vary with the surface loading. At low surface coverage, the isosteric heat is related to the interaction between the adsorbent surface and adsorptive molecular forces.[83] In this range, the pore size can also be an important factor. In the case of zeolites, the results show that the isosteric heat of CO_2 adsorption is very high for the whole range of coverage (28−42 kJ/mol). The slight fluctuations in the heat of adsorption curves could be related to lateral interactions between the adsorbed molecules.[84,85] Related to the high affinity of the zeolites for CO_2 at low pressures, the estimation of the isosteric heat of adsorption at zero loading might have considerable errors and might also explain the significant variation of the reported data.[40] In the case of the activated carbon, the isosteric heat of adsorption decreased with increasing surface loading. This behavior could indicate that energetic heterogeneity arises because of the presence of structural defects and the preferential filling of those sites associated with the strongest electrical field.[86] A similar behavior has also been described by various authors in studies of other types of activated carbon and can be explained in terms of weakly repulsive interactions between adsorbed CO_2 molecules.[87]

Our findings also show that the isosteric heat of adsorption decreases continuously with increasing loading for PILCs. The strong interaction between the large quadrupole moment of CO_2 and alumina and zirconia appears to be the reason for the high isosteric heat of CO_2 adsorption on the pillared clays at low loadings. At higher loadings, the lower-energy sites of the clay are predominantly occupied by CO_2.

In the case of MOFs, the isosteric heats of adsorption are basically constant and can be related to a compensation of the effects of energetic heterogeneity and adsorbate−adsorbate interactions.[64,84] In the case of Z1200, the high isosteric heat can be related to the existence of coordinatively unsatured sites. The isosteric heat of adsorption at zero coverage (by Clausius−Clapeyron equation) shows that the adsorbent−CO_2 affinity increases in the order Z1200 ≈ 13X ≈ 13A < 5A < Zr-PILC < A100 ≈ AC ≈ Al-PILC.

The limiting heat, q_{st}^0, can be obtained directly from the temperature dependence of Henry's constant by applying the Clausius−Clapeyron equation in the low-pressure region, where the isotherm obeys Henry's law[88]

$$q_{st}^0 = R\left[\frac{\mathrm{d}\ln H_i}{\mathrm{d}(1/T)}\right]_{n=0} \tag{11}$$

Under these conditions, the limiting heat of adsorption equals the D_i parameter in the temperature-dependent description of the Henry's constant (see eq 8). The isosteric heats obtained from eqs 8 and 10, as well as the first experimental values included in Figure 3, are compared in Table 3. Literature data are also included in Table 3 for

Table 3. Isosteric Heats of Adsorption at Zero Coverage (q_{st}^0, kJ/mol) for Microporous Materials Obtained Using Four Methods

material	low pressure	virial	Toth	Clausius−Clapeyron	literature
5A	42.81	22.16	50.70	20.79	46[14]
13A	39.03	26.59	41.59	19.98	
13X	26.32	16.52	39.72	19.96	40,[89] 37.2,[40] 49.1[90]
A100	23.93	28.92	22.34	28.60	35,[59] 38.4[91]
Z1200	17.78	17.72	18.78	19.56	17.5−18.5,[92] 15.93[93]
AC	25.21	29.34	34.41	29.77	
Al-PILC	18.49	30.64	92.92	29.92	
Zr-PILC	18.70	25.13	1600	23.59	

comparative purposes. Taking into account the methods used to calculate q_{st}^0, the values obtained for the temperature dependence of the Henry's constant calculated using the virial method were closer to those obtained by the Clausius−Clapeyron equation. The values obtained using the other two methods (low pressure and Toth) were, in general, higher than those obtained using the virial method. However, significant differences between the values obtained using the virial method and the results obtained by the Clausius−Clapeyron equation were only obtained in the case of zeolites 13A and 13X. In the better of our knowledge, the q_{st}^0 previously reported for Z1200 have been obtained only by simulation,[93] and no data have been reported for PILCs.

5. SUMMARY AND CONCLUSIONS

This work has presented a comparative study of the adsorption equilibrium of CO_2 on eight microporous materials at several temperatures in the range of 263−293 K and over a wide range of pressures up to 120 kPa.

It was shown that zeolite 13X exhibits a far better CO_2 adsorption capacity at 273 K and 120 kPa than the other porous materials. The adsorption capacity also increases rapidly for the A100 material, and at high pressures, this material could have the highest adsorption capacity. All of the adsorption data were found to be well-described by the Toth equation, and the Freundlich isotherm can also describe the behavior found for the MOFs, activated carbon, and pillared clays.

Several methods were used herein to calculate the Henry's law constants, with the six-coefficient virial equation being found to be the best method, as it provides an accurate

dx.doi.org/10.1021/ie400380w | Ind. Eng. Chem. Res. 2013, 52, 6785−6793

extrapolation of the adsorption constant at zero coverage. The values found for the zeolites from this method, which ranged from 4.26 to 30.47 mmol/kPa·g, were much higher than those for the metal−organic frameworks, the activated carbon, and the pillared clays, which ranged from 0.007 to 0.200 mmol/kPa·g.

The isosteric heats of CO_2 adsorption on the materials were calculated using the Clausius−Clapeyron equation, and the obtained dependence of the isosteric heats on the amount of CO_2 adsorbed provided insight into the heterogeneity of the materials. Finally, the isosteric heats of adsorption at zero coverage were calculated directly from the temperature dependence of the Henry's constant, thus showing that the adsorbent−CO_2 affinity increases in the order Z1200 ≈ 13X ≈ 13A < 5A < Zr-PILC < A100 ≈ AC ≈ Al-PILC.

■ ASSOCIATED CONTENT

Ⓢ Supporting Information

Additional information as noted in text. This material is available free of charge via the Internet at http://pubs.acs.org.

■ AUTHOR INFORMATION

Corresponding Author

*E-mail: andoni@unavarra.es. Tel.: +34 948 169602.

Notes

The authors declare no competing financial interest.

■ ACKNOWLEDGMENTS

This work was supported by the Spanish Ministry of Economy and Competitiveness (MINECO) through Project PRI-PIBAR-2011-1369. S.G. acknowledges financial support from Public University of Navarra through a Ph.D. fellowship.

■ REFERENCES

(1) *International Energy Outlook*; Report DOE/EIA-0484(2011); U.S. Energy Information Administration: Washington, DC, 2012; available at http://www.eia.gov/forecasts/ieo/pdf/0484(2011).pdf.

(2) Yamasaki, A. An Overview of CO_2 Mitigation Options for Global Warming-Enphazing CO_2 Sequestration Options. *J. Chem. Eng. Jpn.* **2003**, *36*, 361.

(3) Yang, H.; Xu, Z.; Fan, M.; Gupta, R.; Slimane, B.; Bland, A. E.; Wright, I. Progress in Carbon Dioxide Separation and Capture: A Review. *J. Environ. Sci.* **2008**, *20*, 14.

(4) D'Alessandro, D. M.; Smit, B.; Long, J. R. Carbon Dioxide Capture: Prospects for New Materials. *Angew. Chem., Int. Ed.* **2010**, *49*, 6058.

(5) Li, J.-R.; Ma, Y.; McCarthy, M. C.; Sculley, J.; Yu, J.; Jeong, H.-K.; Balbuena, P. B.; Zhou, H.-C. Carbon Dioxide Capture-Related Gas Adsorption and Separation in Metal−Organic Frameworks. *Coord. Chem. Rev.* **2011**, *255*, 1791.

(6) Veawab, A.; Tontiwachwuthikul, P.; Chakma, A. Corrosion Behavior of Carbon Steel in the CO_2 Absorption Process Using Aqueous Amine Solutions. *Ind. Eng. Chem. Res.* **1999**, *38*, 3917.

(7) Rinker, E.; Ashour, S. S.; Sandall, O. C. Absorption of Carbon Dioxide into Aqueous Blends of Diethanolamine and Methyldiethanolamine. *Ind. Eng. Chem. Res.* **2000**, *39*, 4346.

(8) Ruthven, D. M.; Farooq, S.; Knaebel, K. S. *Pressure Swing Adsorption*; John Wiley & Sons: New York, 1993.

(9) Chue, K. T.; Kim, J. N.; Yoo, Y. J.; Cho, S. H.; Yang, R. T. Comparison of Activated Carbon and Zeolites 13X for CO_2 Recovery from Flue Gas by Pressure Swing Adsorption. *Ind. Eng. Chem. Res.* **1995**, *34*, 591.

(10) Ridha, F. N.; Yang, Y.; Webley, P. A. Adsorption Characteristics of a Fully Exchanged Potassium Chabazite Zeolite Prepared from Decomposition of Zeolite Y. *Microporous Mesoporous Mater.* **2009**, *117*, 497.

(11) Gao, W.; Butter, D.; Tomasko, D. L. High-Pressure Adsorption of CO_2 on NaY Zeolite and Model Prediction of Adsorption Isotherms. *Langmuir* **2004**, *20*, 8083.

(12) Siriwardane, R. V.; Shen, M. S.; Fisher, E. P. Adsorption of CO_2 on Zeolites at Moderate Temperatures. *Energy Fuels* **2005**, *19*, 1153.

(13) Walton, K. S.; Abney, M. B.; LeVan, M. D. CO_2 Adsorption in Y and X Zeolites Modified by Alkali Metal Cation Exchange. *Microporous Mesoporous Mater.* **2006**, *91*, 78.

(14) Deng, H.; Yi, H.; Tang, X.; Yu, Q.; Ning, P.; Yang, L. Adsorption Equilibrium for Sulfur Dioxide, Nitric Oxide, Carbon Dioxide, Nitrogen on 13X and 5A Zeolites. *Chem. Eng. J.* **2012**, *188*, 77.

(15) Zukal, A.; Dominguez, I.; Mayerova, J.; Cejka, J. Functionalization of Delaminated Zeolite ITQ-6 for the Adsorption of Carbon Dioxide. *Langmuir* **2009**, *25*, 10314.

(16) Jadhav, P. D.; Chatti, R. V.; Biniwale, R. B.; Labhsetwar, N. K.; Devotta, S.; Rayalu, S. S. Monoethanol Amine Modified Zeolite 13X for CO_2 Adsorption at Different Temperatures. *Energy Fuels* **2007**, *21*, 3555.

(17) Kikkinides, E. S.; Yang, R. T. Concentration and Recovery of CO_2 from Flue Gas by Pressure Swing Adsorption. *Ind. Eng. Chem. Res.* **1993**, *32*, 2714.

(18) Siriwardane, R. V.; Shen, M.-S.; Fisher, E. P.; Poston, J. A. Adsorption of CO_2 on Molecular Sieves and Activated Carbon. *Energy Fuels* **2001**, *15*, 279.

(19) Prezepiorski, J.; Skrodzewicz, M.; Morawski, A. W. High Temperature Ammonia Treatment of Activated Carbon for Enhancement of CO_2 Adsorption. *Appl. Surf. Sci.* **2004**, *225*, 235.

(20) Himeno, S.; Komatsu, T.; Fujita, S. High-Pressure Adsorption Equilibria of Methane and Carbon Dioxide on Several Activated Carbons. *J. Chem. Eng. Data* **2005**, *50*, 369.

(21) Carrott, P. J. M.; Cansado, I. P. P.; Ribeiro Carrott, M. M. L. Carbon Molecular Sieves from PET for Separations Involving CH_4, CO_2, O_2 and N_2. *Appl. Surf. Sci.* **2006**, *252*, 5948.

(22) Heuchel, M.; Davies, G. M.; Buss, E.; Seaton, N. A. Adsorption of Carbon Dioxide and Methane and Their Mixtures on an Activated Carbon: Simulation and Experiment. *Langmuir* **1999**, *15*, 8695.

(23) Harlick, P. J. E.; Sayari, A. Applications of Pore-Expanded Mesoporous Silicas. 3. Triamine Silane Grafting for Enhanced CO_2 Adsorption. *Ind. Eng. Chem. Res.* **2006**, *45*, 3248.

(24) Oliveira, E. L. G.; Grande, C. A.; Rodrigues, A. E. CO_2 Sorption on Hydrotalcite and Alkali-Modified (K and Cs) Hydrotalcites at High Temperature. *Sep. Purif. Technol.* **2008**, *62*, 137.

(25) Yong, Z.; Mata, V.; Rodrigues, A. E. Adsorption of Carbon Dioxide at High Temperature—A Review. *Sep. Purif. Technol.* **2002**, *26*, 195.

(26) Karadas, F.; Yavuz, C. T.; Zulfiqar, S.; Aparicio, S.; Stucky, G. D.; Atilhan, M. CO_2 Adsorption Studies on Hydroxy Metal Carbonates $M(CO_3)_x(OH)_y$ (M═Zn, Zn−Mg, Mg, Mg−Cu, Cu, Ni, and Pb) at High Pressures up to 175 bar. *Langmuir* **2011**, *27*, 10642.

(27) Dietzel, P. D. C.; Besikiotis, V.; Blom, R. Application of Metal−Organic Frameworks with Coordinatively Unsaturated Metal Sites in Storage and Separation of Methane and Carbon Dioxide. *J. Mater. Chem.* **2009**, *19*, 7362.

(28) Millward, A. R.; Yaghi, O. M. Metal−Organic Frameworks with Exceptionally High Capacity for Storage of Carbon Dioxide at Room Temperature. *J. Am. Chem. Soc.* **2005**, *127*, 17998.

(29) Bastin, L.; Brcia, P. S.; Hurtado, E. J.; Silva, J. A. C.; Rodrigues, A. E.; Chen, B. A Microporous Metal−Organic Framework for Separation of CO_2/N_2 and CO_2/CH_4 by Fixed-Bed Adsorption. *J. Phys. Chem. C* **2008**, *112*, 1575.

(30) Sumida, K.; Rogow, D. L.; Mason, J. A.; McDonald, T. M.; Bloch, E. D.; Herm, Z. R.; Bae, T.-H.; Long, J. R. Carbon Dioxide Capture in Metal−Organic Frameworks. *Chem. Rev.* **2012**, *112*, 724.

(31) Sircar, S.; Golden, T. C.; Rao, M. B. Activated Carbon for Gas Separation and Storage. *Carbon* **1996**, *34*, 1.

(32) Sjostrom, S.; Krutka, H. Evaluation of Solid Sorbents as a Retrofit Technology for CO_2 Capture. *Fuel* **2010**, *89*, 1298.
(33) Radosz, M.; Hu, X.; Krutkramelis, K.; Shen, Y. Flue-Gas Carbon Capture on Carbonaceous Sorbents: Toward a Low-Cost Multifunctional Carbon Filter for "Green" Energy Producers. *Ind. Eng. Chem. Res.* **2008**, *47*, 3783.
(34) Shen, W.; He, Y.; Zhang, S.; Li, J.; Fan, W. Yeast-Based Microporous Carbon Materials for Carbon Dioxide Capture. *ChemSusChem* **2012**, *5*, 1274.
(35) Choi, S.; Drese, J. H.; Jones, C. W. Adsorbent Materials for Carbon Dioxide Capture from Large Anthropogenic Point Sources. *ChemSusChem* **2009**, *2*, 796.
(36) Chou, C. T.; Chen, C. Y. Carbon Dioxide Recovery by Vacuum Swing Adsorption. *Sep. Purif. Technol.* **2004**, *39*, 51.
(37) Frere, M.; Weireld, G. P.; Jadot, R. Characterization of Porous Carbonaceous Sorbents Using High Pressure CO_2 Adsorption Data. *J. Porous Mater.* **1998**, *5*, 275.
(38) Mazumder, S.; van Hemert, P.; Busch, A.; Wolf, K.-H. A. A.; Tejera-Cuesta, P. Flue Gas and Pure CO_2 Sorption Properties of Coal: A Comparative Study. *Int. J. Coal Geol.* **2006**, *67*, 267.
(39) Siriwardane, R. V.; Shen, M.-S.; Fisher, E. P.; Poston, J. A. Adsorption of CO_2 on Molecular Sieves and Activated Carbon. *Energy Fuels* **2001**, *15*, 279.
(40) Cavenati, S.; Grande, C. A.; Rodrigues, A. E. Adsorption Equilibrium of Methane, Carbon Dioxide, and Nitrogen on Zeolite 13X at High Pressures. *J. Chem. Eng. Data* **2004**, *49*, 1095.
(41) Mueller, U.; Schubert, M.; Teich, F.; Puetter, H.; Schierle-Arndt, K.; Pastre, J. Metal−Organic Frameworks—Prospective Industrial Applications. *J. Mater. Chem.* **2006**, *16*, 626.
(42) Ferey, G. Hybrid Porous Solids: Past, Present, Future. *Chem. Soc. Rev.* **2008**, *37*, 191.
(43) Wang, Q. M.; Shen, D.; Bulow, M.; Lau, M. L.; Deng, S.; Fitch, F. R.; Lemcoff, N. O.; Semanscin, J. Metallo-Organic Molecular Sieve for Gas Separation and Purification. *Microporous Mesoporous Mater.* **2002**, *55*, 217.
(44) Li, J.-T.; Kuppler, R. J.; Zhou, H.-C. Selective Gas Adsorption and Separation in Metal−Organic Frameworks. *Chem. Soc. Rev.* **2009**, *38*, 1477.
(45) Ma, S.; Zhou, H.-C. Gas Storage in Porous Metal−Organic Frameworks for Clean Energy Applications. *Chem. Commun.* **2010**, *46*, 44.
(46) Banerjee, R.; Phan, A.; Wang, B.; Knobler, C.; Furukawa, H.; O'Keeffe, M.; Yagho, O. M. High-Throughput Synthesis of Zeolitic Imidizolate Frameworks and Application. *Science* **2008**, *319*, 939.
(47) Park, K. S.; Ni, Z.; Côté, A. P.; Choi, J. Y.; Huang, R. D.; Uribe-Romo, F. J.; Chae, H. K.; O'Keeffe, M.; Yaghi, O. M. Exceptional Chemical and Thermal Stability of Zeolitic Imidazolate Frameworks. *Proc. Natl. Acad. Sci. U.S.A.* **2006**, *103*, 10186.
(48) Hayashi, H.; Cote, A. P.; Furukawa, H.; O'Keeffe, M.; Yaghi, O. M. Zeolite A Imidazolate Frameworks. *Nat. Mater.* **2007**, *6*, 501.
(49) Rallapalli, P.; Prasanth, K. P.; Patil, D.; Somani, R. S.; Jasra, R. V.; Bajaj, H. C. Sorption Studies of CO_2, CH_4, N_2, CO, O_2 and Ar on Nanoporous Aluminum Terephthalate [MIL-53(Al)]. *J. Porous Mater.* **2011**, *18*, 205.
(50) Gil, A.; Korili, S. A.; Vicente, M. A. Recent Advances in the Control and Characterization of the Porous Structure of Pillared Clay Catalysts. *Catal. Rev.: Sci. Eng.* **2008**, *50*, 153.
(51) Yang, R. T.; Baksh, M. S. A. Pillared Clays as a New Class of Sorbents for Gas Separation. *AIChE J.* **1991**, *37*, 679.
(52) Pires, J.; Bestilleiro, M.; Pinto, M.; Gil, A. Selective Adsorption of Carbon Dioxide, Methane and Ethane by Porous Clays Heterostructures. *Sep. Purif. Technol.* **2008**, *61*, 161.
(53) Gil, A.; Trujillano, R.; Vicente, M. A.; Korili, S. A. Hydrogen Adsorption by Microporous Materials Based on Alumina-Pillared Clays. *Int. J. Hydrogen Energy* **2009**, *34*, 8611.
(54) García Blanco, A. A.; Vallone, A. F.; Gil, A.; Sapag, K. A Comparative Study of Various Microporous Materials to Store Hydrogen by Physical Adsorption. *Int. J. Hydrogen Energy* **2012**, *37*, 14870.
(55) Hartzog, D. G.; Sircar, S. Sensitivity of PSA Process Performance to Input Variables. *Adsorption* **1995**, *1#2*, 133.
(56) Ahmadpouri, A.; Do, D. D. Isosteric Heat: A Criterion for Equilibrium Model Selection. In *Proceedings of the 2nd Pacific Basin Conference on Adsorption Science and Technology*; Do, D. D., Ed.; World Scientific: Singapore, 2000; p 36.
(57) Baerlocher, Ch.; McCusker, L. B.*Database of Zeolite Structures*; Structure Commission of the International Zeolite Association (IZA), 1996; available at http://www.iza-structure.org/databases (accessed Oct 2012).
(58) Serre, C.; Millange, F.; Thouvenot, C.; Noguès, M.; Marsolier, G.; Louër, D.; Férey, G. Very Large Breathing Effect in the First Nanoporous Chromium(III)-Based Solids: MIL-53 or $Cr^{III}(OH)\cdot\{O_2C-C_6H_4-CO_2\}\cdot\{HO_2C-C_6H_4-CO_2H\}_x\cdot H_2O_y$. *J. Am. Chem. Soc.* **2002**, *124*, 13519.
(59) Bourrelly, S.; Llewellyn, P. L.; Serre, C.; Millange, F.; Loiseau, T.; Férey, G. Different Adsorption Behaviors of Methane and Carbon Dioxide in the Isotypic Nanoporous Metal Terephthalates MIL-53 and MIL-47. *J. Am. Chem. Soc.* **2005**, *127*, 13519.
(60) Gil, A.; Assis, F. C. C.; Albeniz, S.; Korili, S. A. Removal of Dyes from Wastewaters by Adsorption on Pillared Clays. *Chem. Eng. J.* **2011**, *168*, 1032.
(61) Do, D. D. *Adsorption Analysis: Equilibria and Kinetics*; Imperial College Press: London, 1998.
(62) Tóth, F. *Adsorption: Theory, Modelling and Analysis*; Marcel Dekker Inc.: New York, 2002.
(63) Huang, T. Ch.; Cho, L.-T. Relationships Between Constants of the Freundlich Equation and Temperature for Gaseous Adsorption. *Chem. Eng. Commun.* **1989**, *75*, 181.
(64) Ruthven, D. M. *Principles of Adsorption and Adsorption Processes*; John Wiley & Sons: New York, 1984.
(65) Cole, J. H.; Everett, D. H.; Marshall, C. T.; Paniego, A. R.; Powl, J. C.; Rodríguez-Reinoso, F. Physical Chemistry in Condensed Phases. *J. Chem. Soc., Faraday Trans.* **1974**, *70*, 2154.
(66) Bevington, P. R.; Robinson, D. K. *Data Reduction and Error Analysis for the Physical Sciences*, 2nd ed.; McGraw-Hill: New York, 1992.
(67) Gil, A.; Trujillano, R.; Vicente, M. A.; Korili, S. A. Analysis of the Structure of Alumina-Pillared Clays by Nitrogen and Carbon Dioxide Adsorption. *Adsorpt. Sci. Technol.* **2007**, *25*, 217.
(68) Sircar, S. Excess Properties and Thermodynamics of Multicomponent Gas Adsorption. *J. Chem. Soc., Faraday Trans. I* **1985**, *81*, 1527.
(69) Gregg, S. J.; Sing, K. S. W. *Adsorption, Surface Area, and Porosity*; Academic Press: New York, 1991.
(70) Rouquerol, J.; Llewellyn, P.; Rouquerol, F. Is the BET Equation Applicable to Microporous Adsorbents? *Stud. Surf. Sci. Catal.* **2007**, *160*, 49.
(71) Rouquerol, F.; Rouquerol, J.; Sing, K. *Adsorption by Powders and Porous Solids*; Academic Press: San Diego, CA, 1999.
(72) Bhambhani, M. R.; Cutting, P. A.; Sing, K. S. W.; Turk, D. H. Analysis of Nitrogen Adsorption Isotherms on Porous and Nonporous Silicas by the BET and α_s Methods. *J. Colloid Interface Sci.* **1972**, *38*, 109.
(73) Rodriguez-Reinoso, F.; Martin-Martinez, J. M.; Prado-Burguete, C.; McEnaney, B. A Standard Adsorption Isotherm for the Characterization of Activated Carbons. *J. Phys. Chem.* **1987**, *91*, 515.
(74) Dubinin, M. M. Fundamentals of the Theory of Adsorption in Micropores of Carbon Adsorbents: Characteristics of Their Adsorption Properties and Microporous Structures. *Carbon* **1989**, *27*, 457.
(75) Sing, K. S. W.; Everett, D. H.; Haul, R. A. W.; Moscou, L.; Pierotti, R. A.; Rouquerol, J.; Siemieniewska, T. Reporting physisorption data for gas/solid systems with special reference to the determination of surface area and porosity (recommendations 1984). *Pure Appl. Chem.* **1985**, *57*, 603.
(76) Kakei, K.; Ozeki, S.; Suzuki, T.; Kaneko, K. Multi-Stage Micropore Filling Mechanism of Nitrogen on Microporous and Micrographitic Carbons. *J. Chem. Soc., Faraday Trans.* **1990**, *86*, 371.

(77) Ridha, F. N.; Webley, P. A. Anomalous Henry's Law Behaviour of Nitrogen and Carbon Dioxide Adsorption on Alkali-Exchanged Chabazite Zeolite. *Sep. Purif. Technol.* **2009**, *67*, 336.
(78) Palomino, M.; Corma, A.; Rey, F.; Valencia, S. New Insights on CO_2−Methane Separation Using LTA Zeolites with Different Si/Al Ratios and a First Comparison with MOFs. *Langmuir* **2010**, *26*, 1910.
(79) Schell, J.; Casas, N.; Pini, R.; Mazzotti, M. Pure and Binary Adsorption of CO_2, H_2, and N_2 on Activated Carbon. *Adsorption* **2012**, *18*, 49.
(80) Mishra, P.; Mekala, S.; Dreisbach, F.; Mandal, B.; Gumma, S. Adsorption of CO_2, CO, CH_4 and N_2 on a Zinc Based Metal Organic Framework. *Sep. Purif. Technol.* **2012**, *94*, 124.
(81) Shen, Ch.; Grande, C. A.; Li, P.; Yu, J.; Rodrigues, A. E. Adsorption Equilibria and Kinetics of CO_2 and N_2 on Activated Carbon Beads. *Chem. Eng. J.* **2010**, *160*, 398.
(82) Xu, X.; Zhao, X.; Sun, L.; Liu, X. Adsorption Separation of Carbon Dioxide, Methane, and Nitrogen on Hβ and Na-Exchanged β-Zeolite. *J. Nat. Gas Chem.* **2008**, *17*, 391.
(83) Nguyen, C.; Do, D. D. Adsorption of Supercritical Gases in Porous Media: Determination of Micropore Size Distribution. *J. Phys. Chem. B* **1999**, *103*, 6900.
(84) Auerbach, S. M.; Carrado, K. A.; Dutta, P. B. *Handbook of Zeolite Science and Technology*; Marcel Dekker, Inc.: New York, 2003.
(85) Bottani, E. J.; Bakaev, V.; Steele, W. A Simulation/Experimental Study of the Thermodynamic Properties of Carbon Dioxide on Graphite. *Chem. Eng. Sci.* **1994**, *49*, 2931.
(86) Barrer, R. M.; Wasilewski, S. *Trans. Faraday Soc.* **1961**, *57*, 1141.
(87) Guo, B.; Chang, L.; Xiel, K. Adsorption of Carbon Dioxide on Activated Carbon. *J. Nat. Gas Chem.* **2006**, *15*, 223.
(88) Sircar, S. Estimation of Isosteric Heats of Adsorption of Single Gas and Multicomponent Gas Mixtures. *Ind. Eng. Chem. Res.* **1992**, *31*, 1813.
(89) Lee, J.-S.; Kim, J.-H.; Kim, J.-T.; Suh, J.-K.; Lee, J.-M.; Lee, C.-H. Adsorption Equilibria of CO_2 and Zeolite X/Activated Carbon Composite. *J. Chem. Eng. Data* **2002**, *47*, 1237.
(90) Dunne, J. A.; Rao, M.; Sircar, S.; Gorte, R. J.; Myers, A. L. Calorimetric Heats of Adsorption and Adsorption Isotherms. 2. O_2, N_2, Ar, CO_2, CH_4, C_2H_6, and SF_6 on NaX, H-ZSM-5, and Na-ZSM-5 Zeolites. *Langmuir* **1996**, *12*, 5896.
(91) Couck, S.; Denayer, J. F. M.; Baron, G. V.; Rémy, T.; Gascon, J.; Kapteijn, F. An Amine-Functionalized MIL-53 Metal−Organic Framework with Large Separation Power for CO_2 and CH_4. *J. Am. Chem. Soc.* **2009**, *131*, 6326.
(92) Huang, H.; Zhang, W.; Liu, D.; Liu, B.; Chen, G.; C. Zhong, C. Effect of Temperature on Gas Adsorption and Separation in ZIF-8: A Combined Experimental and Molecular Simulation Study. *Chem. Eng. Sci.* **2011**, *66*, 6297.
(93) Perez-Pellitero, J.; Amrouche, H.; Siperstein, F. R.; Pirngruber, G.; Nieto-Draghi, C.; Chapalis, G.; Simon-Masseron, A.; Bazer-Bachi, D.; Peralta, D.; Bats, N. Adsorption of CO_2, CH_4, and N_2 on Zeolitic Imidazolate Frameworks: Experiments and Simulations. *Chem.—Eur. J.* **2010**, *16*, 1560.

■ NOTE ADDED AFTER ASAP PUBLICATION

This paper posted to the Web on May 10, 2013, with an error to Section 4.1. The corrected version posted online with the Issue on May 22, 2013.